Modeling and Optimization of a High-T_c Hot-Electron Superconducting Mixer for Terahertz Applications

B.S. Karasik[a], W.R. McGrath, M.C. Gaidis, M.J. Burns,

A.W. Kleinsasser, K.A. Delin, R.P. Vasquez

Center for Space Microelectronics Technology, Jet Propulsion Laboratory,

California Institute of Technology, Pasadena, CA 91109

Abstract

The development of a $YBa_2Cu_3O_{7-\delta}$ (YBCO) hot-electron bolometer (HEB) quasioptical mixer for a 2.5 THz heterodyne receiver is discussed. The modeled device is a submicron bridge made from a 10 nm thick film on a high thermal conductance substrate. The mixer performance expected for this device is analyzed in the framework of a two-temperature model which includes heating both of the electrons and the lattice. Also, the contribution of heat diffusion from the film through the substrate and from the film to the normal metal contacts is evaluated. The intrinsic conversion gain and the noise temperature have been calculated as functions of the device size, substrate material, and ambient temperature. Assuming energy fluctuations and Johnson noise to be the main sources of noise, a single sideband (SSB) mixer noise temperature of less than 2000 K is predicted. For our modeled device, the conversion efficiency at an IF of 2.5 GHz is −10 dB or better and the required local oscillator (LO) power is less than 5 μW.

I. Introduction

The superconductive HEB is presently considered the most promising heterodyne mixer device for the terahertz frequency range. Recent experiments with a Nb HEB mixer demonstrated a 560 K DSB noise temperature at 533 GHz and should remain relatively low for rf up to ≈ 10 THz [1]. This type of mixer can

---

[a] E-mail: karasik@kbs-mac.jpl.nasa.gov

be especially useful in space-borne applications for atmospheric research if operated at elevated temperatures where low-power mechanical cryocoolers are readily available and where requirements for a low LO power are critical. For such an application, a HEB device made from a thin YBCO film can be used. The fabrication technology for such films has been significantly improved since the discovery of high-T_c superconductivity. Now, ultrathin films having a thickness d down to a few unit cells have been successfully fabricated [2–6]. The critical temperature $T_c > 85$ K and superconducting transition width $\delta T_c = 1$–2 K are typical for films with $d \geq 10$ nm, and a critical current density $j_c = 8 \times 10^6$ A/cm^2 was observed in 10 nm thick films at 77 K [6]. Fabrication of superconducting structures made from YBCO with in-plane sizes 100–500 nm has also been demonstrated [7–11]. Critical current densities as large as 5×10^6 A/cm^2 have been measured in 200 nm wide superconducting lines [12]. A variety of materials (e.g. MgO, LaAlO$_3$, NdGaO$_3$, YSZ) have been found to provide a moderate dielectric constant and epitaxial YBCO film growth. Also, the use of buffer layers allows growth of YBCO films on silicon and sapphire (YSZ buffer layer for Si and CeO$_2$ for sapphire). With such promising film growth technology, it becomes important for us to now examine the theoretical issues involved in designing optimum devices.

In contrast to slow bulk bolometric detectors, a HEB mixer can operate with a high intermediate frequency (IF) of the order of several gigahertz, and under appropriate LO power (typically of order of μW for sibmicron devices). This sets quite different from detector device criteria for mixer device optimization. In this paper we give a detailed analysis of the thermal processes important for good HEB mixer performance. Within the framework of a model which includes the temperature of both the electrons and phonons, expressions for mixer conversion efficiency, and IF impedance have been derived and analyzed at $f_{IF} = 2.5$ GHz. The contributions of both electron temperature fluctuations and Johnson noise in the mixer noise temperature have been investigated as functions of dc and LO power. Also, the requirements for the substrate thermal conductivity in relationship to the device in-plane size have been determined. A SSB noise temperature ≤ 2000 K should be achievable for an optimized device.

The model developed here is required for optimization of a YBCO HEB mixer for potential use in a heterodyne receiver to observe OH at 2512 GHz in the upper atmosphere. This receiver is part of NASA's Earth Observing System Microwave Limb Sounder instrument. An IF of 2.5 GHz is desired to simultaneously observe the doublet OH lines. The mixer will employ a planar twin-slot antenna on an elliptical silicon lens. A complete description of the experimental details will be given at a later date.

II. Nonequilibrium Photoresponse and Thermal Relaxation in YBCO Films.

The origin of a fast non-equilibrium photoresponse in high-T_c YBCO films has been studied for a number of years. Recent time-domain [13] and frequency-domain [14,15] measurements demonstrate that the resistive response to radiation can be adequately described in terms of relaxation of the electron temperature T_e via interaction with phonons with a characteristic time τ_e of 1–2 ps at 80–90 K, and of a slower relaxation of the phonon temperature T_p. The time constant of the latter quantity depends on the film size and substrate material. One should point out that the mixer response time in a low-T_c HEB is determined by τ_e only, since the escape time for phonons in ~10 nm thick films is much shorter, i.e. the phonons remain in equilibrium with a heat sink.

The principal heat removal processes for a high-T_c device are shown in a flow diagram in Fig. 1. The nonequilibrium electrons heated by the absorbed rf radiation and dc transport current give their energy to phonons during a very short electron-phonon energy relaxation time $\tau_e \approx 1$–2 ps. The electron diffusion mechanism of heat transport which is especially important in submicron Nb HEB mixers [1] is much less significant in YBCO films. Even a very optimistic estimate of the electron diffusivity $D \approx 0.015$ cm^2/s [16] (this is a typical experimental value of a total diffusivity in the a–b plane of oriented YBCO films at 90 K) gives a corresponding diffusion length $l_d \cong \pi\sqrt{D\tau_e} \approx 5$–6 nm, which is much smaller than any realistic device size.

The nonequilibrium phonons leave the film either through the film-substrate boundary or by diffusing to the normal metal contacts. The phonon escape to the substrate is influenced by an acoustic mismatch, i.e., by the thermal boundary resistance $R_b = \tau_{es}/(c_p d)$, where τ_{es} is the phonon escape time and c_p is the phonon specific heat per unit volume. The value of R_b is fairly constant in the temperature range 70–100 K and has been measured for various substrates. One of the lowest reported values of R_b is 5×10^{-4} cm^{2}K/W for MgO substrates [16,17], giving $\tau_{es} \approx 33d$ ps for d in nm. Such values of τ_{es} have been directly measured in a number of experiments [15-19]. The diffusion time of phonons to the contacts can be estimated as $\tau_{dif} \approx L^2/(\pi^2 D)$, where L is the device length. One can see that $\tau_{diff} \cong \tau_{es}$ when $L \approx 0.1$ μm

and $d \approx 10$ nm. For longer samples the diffusion time increases rapidly. In general, the effective time of phonon escape is $\tau_{eff} = \left(\tau_{es}^{-1} + \tau_{dif}^{-1}\right)^{-1}$.
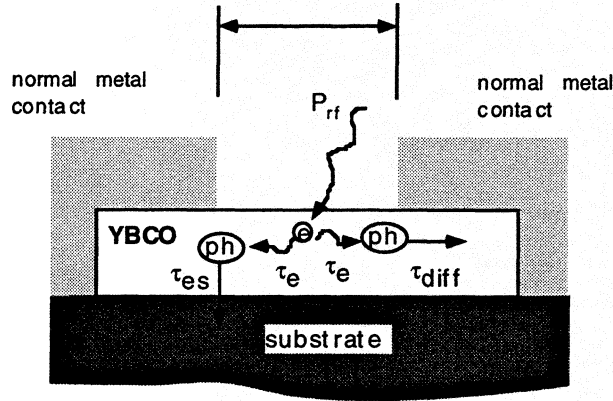

Fig. 1. Flow-diagram of elementary processes in YBCO film: electrons (e) absorbing rf power P_{rf} couple to phonons (ph) during τ_e, then phonons can either diffuse to the contacts or escape to the substrate and diffuse away.

Yet another thermal process affecting the microbridge thermal relaxation speed and the total thermal resistance is the diffusion of heat in the substrate. If the characteristic in-plane device size L is chosen to be much smaller than the substrate thickness d_s, the effective thermal resistance of the substrate is found as [20]:

$$R_s = \left\{ \frac{S\kappa_s}{a} \sqrt{\left[1 + \frac{a}{l_s(f)}\right]^{-1} + \left[\frac{a}{l_s(f)}\right]^{-1}} \right\}^{-1}, \tag{1}$$

where κ_s is the thermal conductivity of the substrate, a is the equivalent radius of the device area through which heat flows into the substrate, $l_s = \sqrt{D_s/(\pi f)}$ is the effective length of diffusion at modulation frequency f, D_s is the phonon diffusivity of the substrate, and S is the device area. For a device with a square shape and a side L, $a = L/\sqrt{\pi}$. Although the total thermal resistance, R_s, decreases, the thermal resistance per unit area, R_s/L^2, becomes larger if the device has larger area.

The optimization of the total thermal resistance between an electron subsystem and a heat sink as well as its modulation frequency dependence is quite important for the HEB mixer operation. A rule of thumb is that the thermal resistance should be made as low as possible and its frequency dependence should be as flat as possible. The minimum thermal resistance determines the maximum LO power contributing to the IF signal. A pronounced frequency dependence of the thermal resistance generally yields a loss of power at the IF of interest with respect to the maximum attainable conversion efficiency at a zero IF. The contributions from thermal boundary resistance and from the substrate will be compared in the following section.

III. Conversion Gain and IF Impedance in a Two-Temperature Model.

In contrast to a low-T_c HEB mixer, a high-T_c HEB mixer cannot be described in terms of the electron temperature only. This is because at temperatures ~ 90 K the phonon heat capacity is always much larger than that of the electrons. A more appropriate approach [21] makes use of a "two-temperature" model describing the dynamics of the electron and phonon temperatures which are both different from the temperature of the heat sink. This is the approach we use here.

The coupled differential equations for the electron and phonon temperatures are given in [22]. The following spectrum of the electron temperature was obtained:

$$\Delta T_e = \alpha P_{rf} \frac{\tau_e + (c_e/c_p)\tau_{es}}{c_e} \sqrt{\frac{1+(\omega\tau_\varphi)^2}{\left[1+(\omega\tau_1)^2\right]\left[1+(\omega\tau_2)^2\right]}}, \tag{2}$$

where α is the rf coupling factor, P_{rf} is the amplitude of the incident rf power, and c_e is the electron specific heat of the film. τ_φ, τ_1, and τ_2 are given by the following formulas:

$$\tau_{1,2}^{-1} = \tau_{+,-}^{-1} = \frac{1}{2\tau}\left(1\pm\sqrt{1-4\frac{\tau^2}{\tau_e\tau_{es}}}\right), \quad \tau^{-1} = \tau_{es}^{-1} + \tau_e^{-1} + \tau_p^{-1}, \quad \tau_\varphi^{-1} = \tau_{es}^{-1} + \tau_p^{-1}, \quad \tau_p = \tau_e c_p/c_e. \tag{3}$$

In YBCO τ_e is so short that $\tau_p \ll \tau_{es}$. This condition, along with $c_p \gg c_e$, allows one to simplify Eqn's. 3:

$$\tau_1 \approx \tau_e, \quad \tau_2 \approx \tau_{es}, \quad \tau_\varphi \approx \tau_p \tag{4}$$

and obtain the following spectrum of the electron temperature:

$$\Delta T_e \approx \alpha P_{rad} \frac{\tau_e + \left(c_e/c_p\right)\tau_{es}}{c_e} \sqrt{\frac{1+\left(\omega\tau_p\right)^2}{\left[1+\left(\omega\tau_e\right)^2\right]\left[1+\left(\omega\tau_{es}\right)^2\right]}} . \tag{5}$$

This frequency dependence for a response in thin YBCO films was observed in recent optical mixing experiments at $\lambda = 1.54$ μm [21] and $\lambda = 9.6$ μm [23].

From Eq. 5 one can obtain the effective thermal resistance between electrons and substrate:

$$R_{e-s} = \frac{\tau_e + \left(c_e/c_p\right)\tau_{es}}{c_e V} \sqrt{\frac{1+\left(\omega\tau_p\right)^2}{\left[1+\left(\omega\tau_e\right)^2\right]\left[1+\left(\omega\tau_{es}\right)^2\right]}} = \left[\tau_e/(c_e V) + R_b/S\right] \sqrt{\frac{1+\left(\omega\tau_p\right)^2}{\left[1+\left(\omega\tau_e\right)^2\right]\left[1+\left(\omega\tau_{es}\right)^2\right]}} , \tag{6}$$

and the total thermal resistance to the bath is

$$R_{tot} = R_{e-s} + R_s. \tag{7}$$

Figure 2 shows the behavior of R_s, R_{e-s} and R_{tot} for two widely used substrates (MgO and LaAlO$_3$) and two device sizes ($L = 10$ μm and $L = 1$ μm). The YBCO film thickness is 10 nm in all cases. Rs dominates for poor thermal conducting substrate, large device sizes, and low IF (e.g. LaAlO$_3$ for $L = 10$ μm). We should point out that Eq. 7 underestimates the total thermal resistance since the reverse flow of phonons from the substrate to the YBCO film is not taken into account. The effect should be larger for larger device areas and lower substrate thermal conductivity. Nevertheless, it is believed that MgO substrates, where $R_s \ll R_{e-s}$, are nearly ideal. R_s becomes negligible for submicron-size devices and will not be considered in the following analysis. We will also not consider the heat diffusion to the contacts. This

process can reduce the total thermal resistance of a 0.1 µm long device. However, even without this mechanism good mixer performance is predicted.

Table I. Physical parameters of YBCO and some substrates at ~ 90 K.

	YBCO	MgO	LaAlO$_3$	YSZ	sapphire	YAlO$_3$
c_e, J K^{-2} cm^{-3}	0.025	–	–	–	–	
c_p, J K^{-2} cm^{-3}	0.64	0.53	0.40	0.70	0.39	
κ, W K^{-1} cm^{-1}	0.015	3.4	0.35	0.015	6.4	0.2-0.4 [a]
R_b, K cm^2 W^{-1}	–	5.0×10^{-4}	1.0×10^{-3}	N/A	1.1×10^{-3}	
ε_r		10	24	28	11	16
tan δ		7×10^{-6}	5×10^{-6}	4×10^{-4}	8×10^{-6}	1×10^{-5}

[a] this work

For use in a practical 2.5 THz receiver, the substrate must also exhibit low rf absorption. We have measured MgO, YAlO3 and sapphire at 77 K in a Fourier transform spectrometer and found them to have acceptable rf transparency. The physical constants for YBCO and a number of useful substrates at 90 K are given in Table 1.

Equations 2 and 5 were obtained assuming no self-heating effects in the superconducting film (small dc current) and a simple, linear (with respect to the electron temperature shift) dependence for the heat flow from electrons to phonons. The latter assumption is applicable for only small differences between T_e and T_p. It has been found experimentally that in YBCO films, $\tau_e \sim T^{-1}$ [24], hence the heat flow from electrons to phonons is actually proportional to $(T_e^3 - T_p^3)$.

Here we discuss the more realistic situation where the device is so far from equilibrium that one can neglect neither the non-linearity in the heat conductance (strong pumping), nor the self-heating caused by transport current. We also include in the model the feedback effect from the IF load influencing the conversion mixer gain and modifying the mixer bandwidth [25].
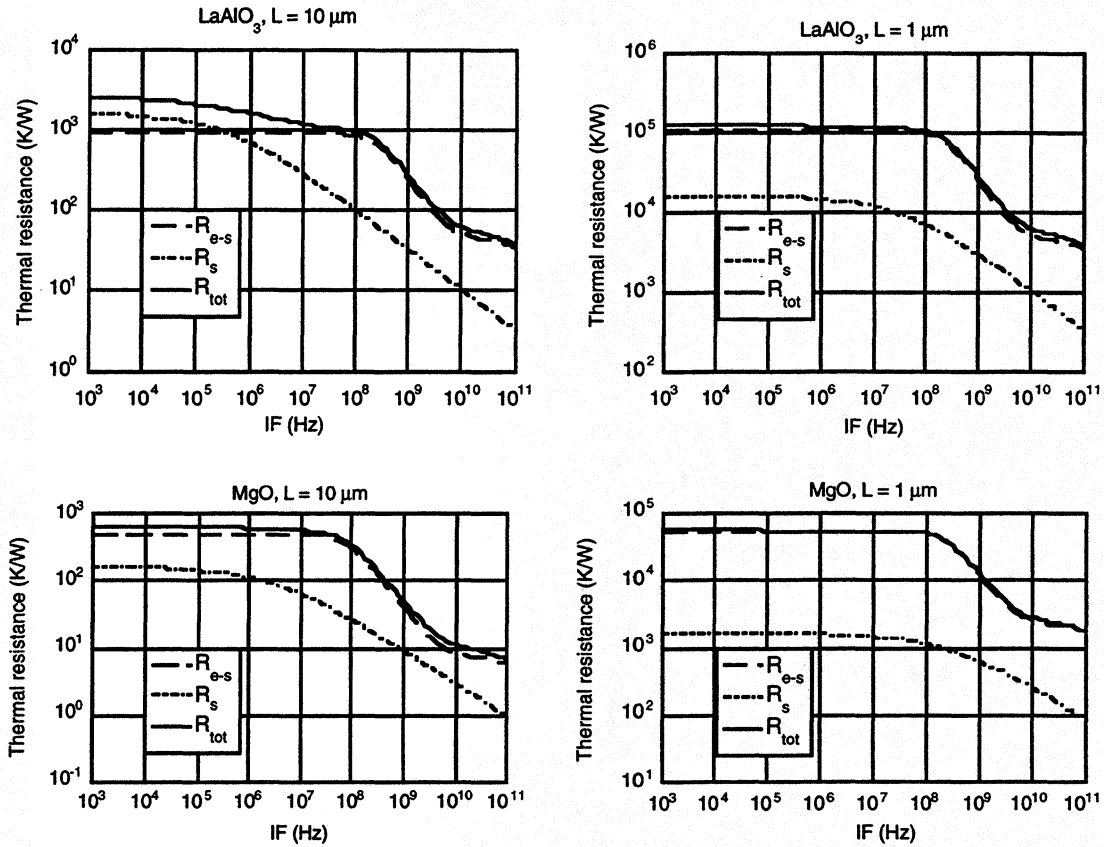
Fig 2. Thermal resistance in a YBCO film-substrate system.

We start with the following dynamic equations:

$$c_e V_d \frac{dT_e}{dt} = -A V_d \left(T_e^3 - T_p^3\right) + I V_b + \alpha P \tag{8a}$$

$$c_p V_d \frac{dT_p}{dt} = A V_d \left(T_e^3 - T_p^3\right) - \frac{S}{R_b}\left(T_p - T\right). \tag{8b}$$

Here V_d is the volume of the microbridge, A is the constant characterizing the strength of the electron-phonon coupling, which scales as $A = \gamma/(\tau_e 3T)$ (γ is the Sommerfeld constant), and V_b an I are the bias voltage and current, respectively. Since we are interested in a periodic solution, the following substitutions can be made $P = P_0 + \tilde{P}e^{j\omega t}$, $T_e = T_{e0} + \tilde{T}_e e^{j\omega t}$, $T_p = T_{p0} + \tilde{T}_p e^{j\omega t}$, $V_b = V_{b0} + \tilde{V}_b e^{j\omega t}$, $I = I_0 + \tilde{I}e^{j\omega t}$,

572

$R = R_0 + \tilde{R}e^{j\omega t}$ where $\tilde{P}$, $\tilde{T}_e$, $\tilde{T}_p$, $\tilde{V}_b$, $\tilde{I}$, and $\tilde{R}$ are the complex amplitudes of the corresponding quantities. Eqn's. 8 is now split into two systems:

for the dc values

$$-AV_d\left(T_{e0}^3 - T_{p0}^3\right) + I_0 V_{b0} + \alpha P_0 = 0 \tag{9a}$$

$$AV_d\left(T_{e0}^3 - T_{p0}^3\right) - \frac{S}{R_b}\left(T_{p0} - T\right) = 0, \tag{9b}$$

and for the 1st harmonics

$$\left(j\omega c_e + 3AT_{e0}^3\right)V_d\tilde{T}_e = 3AV_dT_{p0}^3\tilde{T}_p + I_0\tilde{V}_b - V_{b0}\tilde{I} + \alpha\tilde{P} \tag{10a}$$

$$\left(j\omega c_p + c_p/\tau_{es} + 3AT_{p0}^3\right)\tilde{T}_p = 3AT_{e0}^3\tilde{T}_e. \tag{10b}$$

Substituting $\tilde{T}_p$ from Eq. 10b into Eq. 10a we obtain:

$$3AV_dT_{eo}^2\left[j\omega\tau_e + 1 - \frac{\left(T_{p0}/T_{e0}\right)^2}{j\omega\tau_p + \tau_p/\tau_{es} + \left(T_{p0}/T_{e0}\right)^2}\right]\frac{\tilde{T}_e}{\tilde{P}} = I_0\frac{\tilde{V}_b}{\tilde{P}}\left(1 - R_0/R_L\right) + \alpha, \tag{11}$$

where $R_L = \tilde{V}_b/\tilde{I}$ is the IF load resistance, and $R_0 = V_{b0}/I_0$ is the dc resistance of the device. Using the relationships: $\tilde{V}_b(1 + R_0/R_L) = I_0\tilde{R}$ and $\tilde{R} = (\partial R/\partial Te)\tilde{T}_e$ one can also show that $\tilde{T}_e = \tilde{V}_b(1 + R/R_L)/(I_0\partial R/\partial T_e)$. Then the expression for the HEB detector voltage responsivity can be obtained:

$$S_V \equiv \tilde{V}_b/\tilde{P} = \frac{\alpha C}{I_0}\frac{R_L}{R_L + R_0}\frac{1 + j\omega\tau_0}{\left[\tau_0/\tau_{es} - \omega^2\tau_e\tau_0 + j\omega(\tau_e + \tau_0)\right] + C\dfrac{R_0 - R_L}{R_0 + R_L}(1 + j\omega\tau_0)}. \tag{12}$$

The SSB mixer conversion efficiency is

$$\eta = \frac{2\left|S_V\right|^2 P_{LO}}{R_L} = \frac{2\alpha^2C^2P_{LO}}{P_{DC}}\frac{R_0R_L}{\left(R_0 + R_L\right)^2}\left|\frac{1 + j\omega\tau_0}{\left[\tau_0/\tau_{es} - \omega^2\tau_e\tau_0 + j\omega(\tau_e + \tau_0)\right] + C\dfrac{R_0 - R_L}{R_0 + R_L}(1 + j\omega\tau_0)}\right|^2 .\tag{13}$$

One can verify that in the low temperature limit, when $\tau_{es} \ll \tau_p \ll \tau_e$, the frequency dependent term in the product given by Eq. 13 is reduces to $|1+j\omega\tau_e/[1+C(R_0-R_L)/(R_0+R_L)]|^{-2}$, giving the expression previously obtained in [25].

Postulating that the IF impedance $Z(\omega) = R_0 + (\partial R/\partial T_e)\tilde{T}_e$, and using Eqn's. 8, one can obtain

$$\tilde{Z}(\omega) = R\frac{\left[\tau_0/\tau_{es} - \omega^2\tau_e\tau_0 + j\omega(\tau_e + \tau_0)\right] + C(1 + j\omega\tau_0)}{\left[\tau_0/\tau_{es} - \omega^2\tau_e\tau_0 + j\omega(\tau_e + \tau_0)\right] - C(1 + j\omega\tau_0)},$$

(14)

which coincides in the low-temperature limit with the following expression from [26]:

$$\tilde{Z}(\omega) = R\frac{1+C}{1-C}\frac{1 + j\omega\dfrac{\tau_e}{1+C}}{1 + j\omega\dfrac{\tau_e}{1-C}}.$$

(15)

IV. Noise Temperature.

The expression for the noise temperature due to the electron temperature fluctuations of a low-T_c HEB mixer was given in [26]. It was also shown that this quantity does not depend on the conversion gain, i.e. it is fairly universal. We believe it is applicable for a high-T_c HEB mixer, and the corresponding SSB noise temperature contribution is given by:

$$T_m^{TF} = \frac{2T_e^2 G_e}{\alpha^2 P_{LO}},$$

(16)

where $G_e = 3AV_dT_e^2$ is the thermal conductance between electrons and phonons.

The contribution of Johnson noise should be evaluated by taking into account the enhancement of the noise due to the self-heating in a bolometer. Simply, one can use the equivalent noise circuit introduced in [27] (see Fig. 3). Following [26,27], we assume that the classical Johnson noise source $e_J = \sqrt{4k_BRT_e}$ must appear twice in the bolometer equivalent circuit. Source $E1 = e_J$ acts simply as a voltage source in

series with the bolometer impedance $Z(\omega)$. The source $E2 = -e_J/2$ is placed to take into account the output noise enhancement caused by the self-detection of the Johnson noise in the bolometer. The impedance Z_x represents the bolometer reactance due to its thermal inertia and self-heating contribution. Z_x is chosen to agree with Eq. 14 for the bolometer IF impedance. After passing the frequency dependent impedance Z_x a "white" noise e_J becomes frequency dependent at the load R_L. The corresponding expression for the noise temperature is obtained by dividing the noise power dissipated in the load by the conversion gain given in Eq. 13. A relatively simple expression has been obtained for a low-T_c HEB mixer [26]. However, for the high-T_c case the expression turns to be very cumbersome, therefore we just calculate the noise temperature numerically.
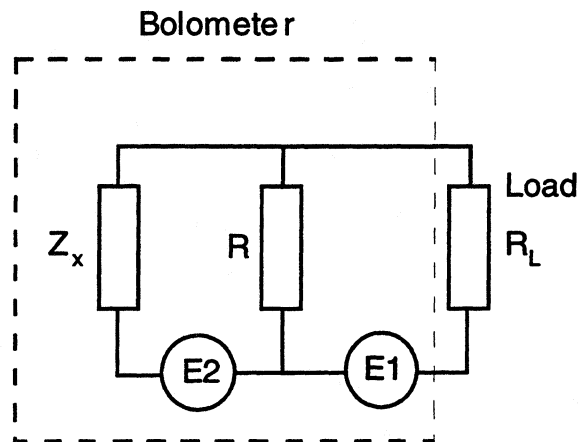
Bolometer

Fig. 3. Equivalent circuit for calculations of the Johnson noise temperature in a bolometer.

V. Numerical Results.

Contour plots in Fig. 4 represent the results of simulations of the HEB mixer SSB noise temperature, T_M (Fig. 4a), and its components: due to electron temperature fluctuations, T_M^{TF} (Fig. 4b), and due to Johnson noise T_M^J (Fig. 4c) at $f_{IF} = 2.5$ GHz. Parameters are chosen which represent realistic estimates for a device to be used in practical cryocooled mixer applications: an area of 0.1×0.1 μm^2, a thickness of 10 nm, $T_c = 85$ K, $\delta T_c = 2$ K, normal resistance $R_n = 400$ Ω, and an operating temperature of $T = 66$ K. A coupling factor α was chosen to be 1 for simplicity (α will depend on the details of the

planar antenna and optics), so P_{LO} designates the absorbed LO power. Figure 4d shows the SSB mixer conversion efficiency under the same conditions, and Fig. 4e shows the device dc resistance. The contours in Figs. 4 are plotted versus dc and LO power since these are two important and experimentally variable parameters for a planar mixer. With the given dc and LO power scales, the top right corner of all plots corresponds to the normal state, the bottom left corner corresponds to a nearly superconducting state. At both of these edges the noise temperature is very high. In the superconducting state, where the LO power is low, T_M^{TF} is high. In the normal state, where the conversion loss is very high, T_M^J is high. Just at the middle of the resistive transition, the noise temperature reaches its minimum value (~1000 K). Figure 5 shows the behavior of the noise temperature in the vicinity of the minimum. Figure 6a shows the IF spectra of the conversion gain and the IF impedance. It is interesting to point out that a negative differential dc resistance Z_0 turns into positive real impedance of about 230 Ω at 2.5 GHz. The conversion efficiency at this frequency is still high (+ 0.36 dB). The combination of the parameters at the optimum point is given in Table 2 (point 1). Negative resistance is not a necessary condition for high conversion efficiency or low noise temperature. For example, the operating point at slightly higher LO power (just above the middle of the superconducting transition) yields a 1300 K noise temperature (Table 2, point 2) and a positive real part of the IF impedance at all frequencies (see Fig. 6b).

Our model does not predict any degradation of the device noise performance if the device size L is made larger. The only parameters which change are LO power and dc power. They simply scale as the device area, i.e. $P_{LO}^{opt} \approx 200L^2$ μW (L is in nm). The effect of the device thickness is more complicated, since not only the dissipated power, but also the total thermal resistance is being changed with the thickness. Figure 7 shows the dependence of the minimum noise temperature vs device thickness. The device area is 0.1×0.1 μm^2 and the normal resistance increases as $1/d$. One can see that T_M is an almost linear function of d, whereas P_{LO} saturates with thickness. This is because T_e-T_p becomes smaller for larger d (see Eq. 8b), and, therefore, the total thermal resistance is dominated by phonon escape (i.e. by R_b). It means that for large thickness, an optimal mixing electron temperature is reached with the same power dissipated in the device. In this case the shift of electron temperature caused by LO power is very small and the optimal LO power is determined by only thermal boundary resistance R_b and does not depend on d.
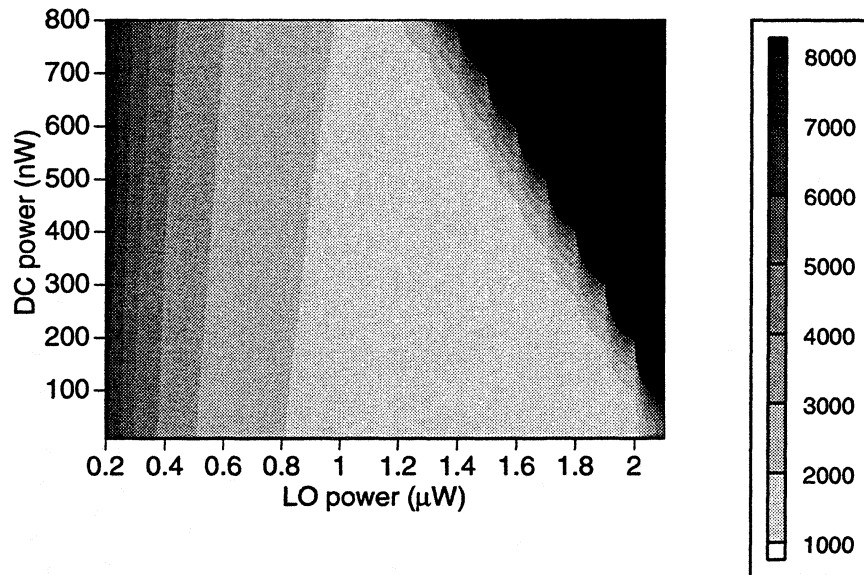
Fig. 4a. Total mixer noise temperature T_M (K). Waviness is an artifact of numerical precision in the simulations
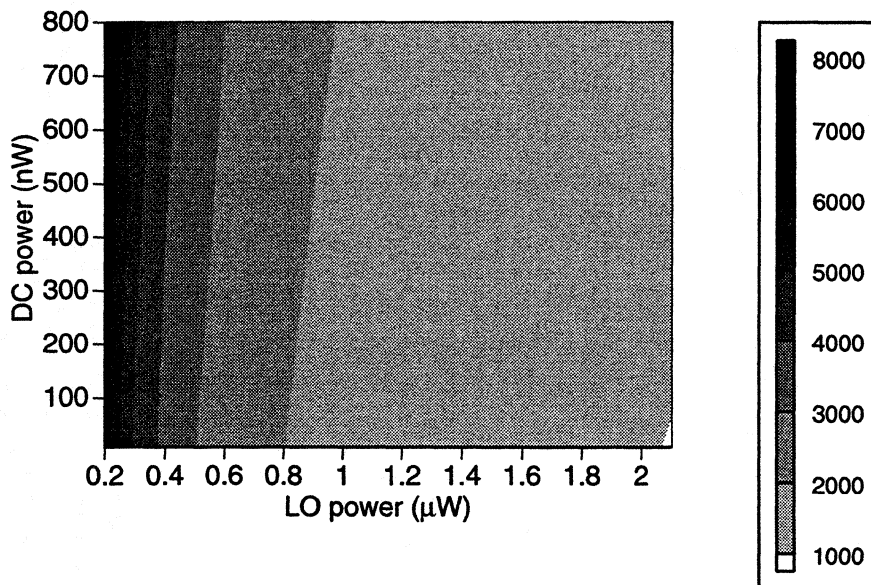

Fig. 4b. Noise temperature contribution due to electron temperature fluctuations T_M^{TF} (K).
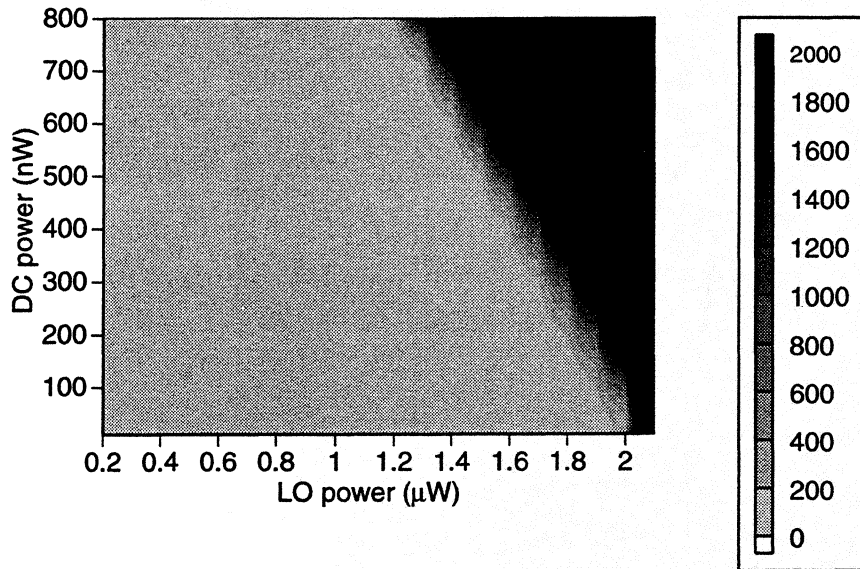
Fig. 4c. Noise temperature contribution due to Johnson noise T_M^J (K). Waviness is an artifact of numerical precision in the simulations
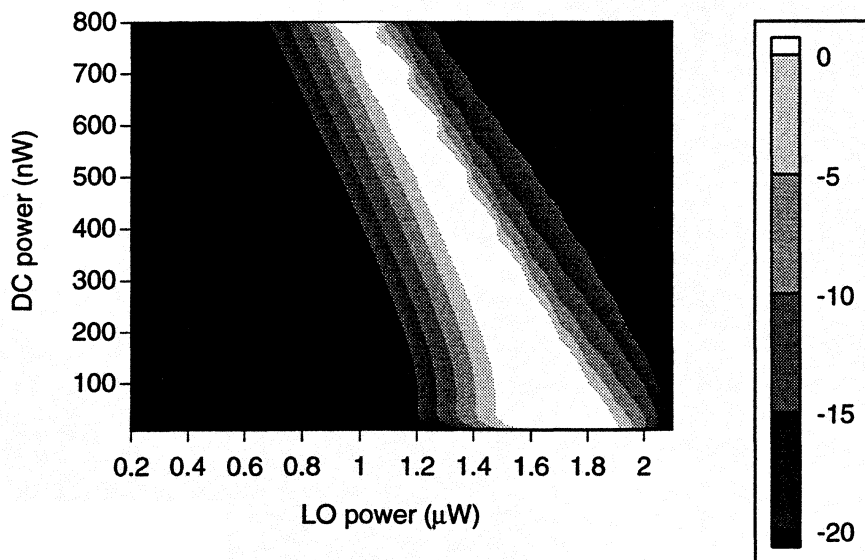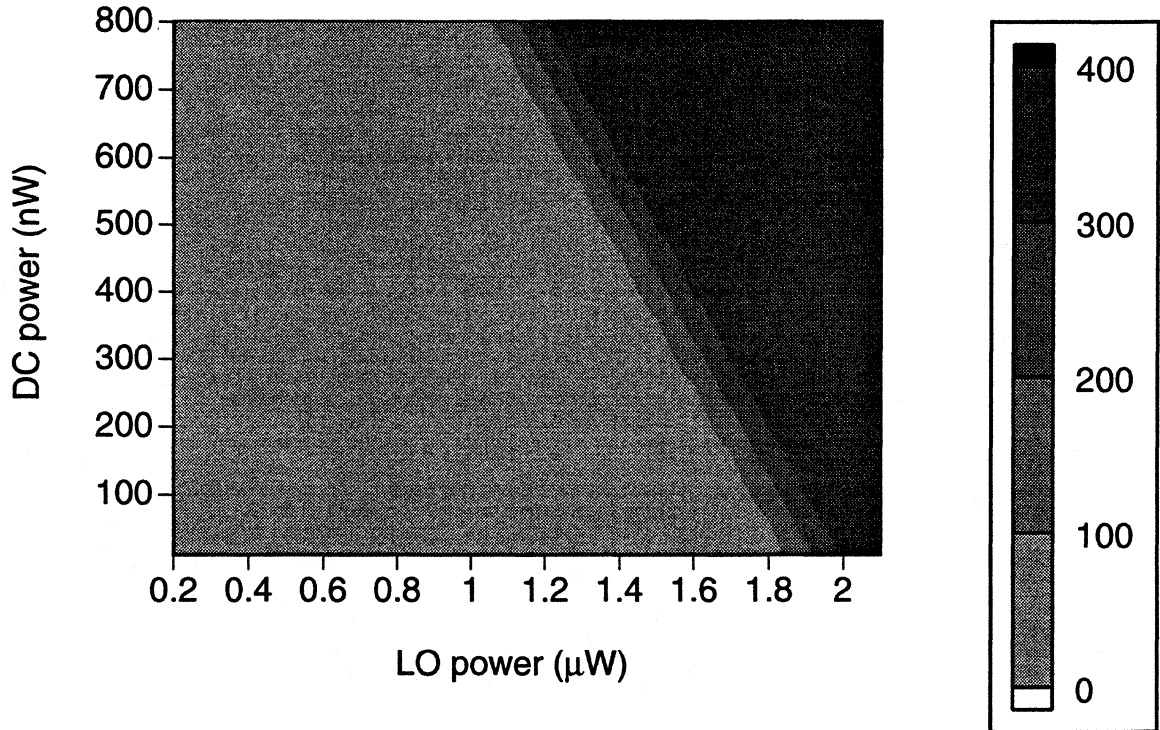

Fig. 4d. Mixer conversion efficiency (dB).
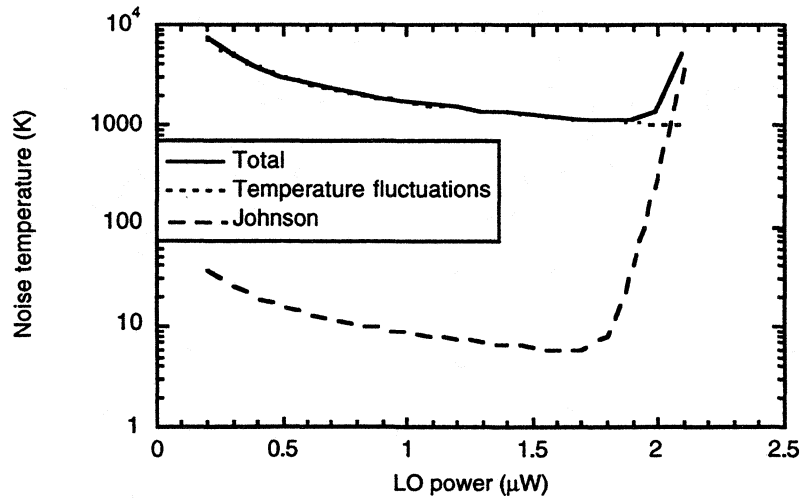
Fig. 4e. Mixer device dc resistance (Ω).

Fig. 5. Noise temperature as a function of LO power in the vicinity of the optimum point.
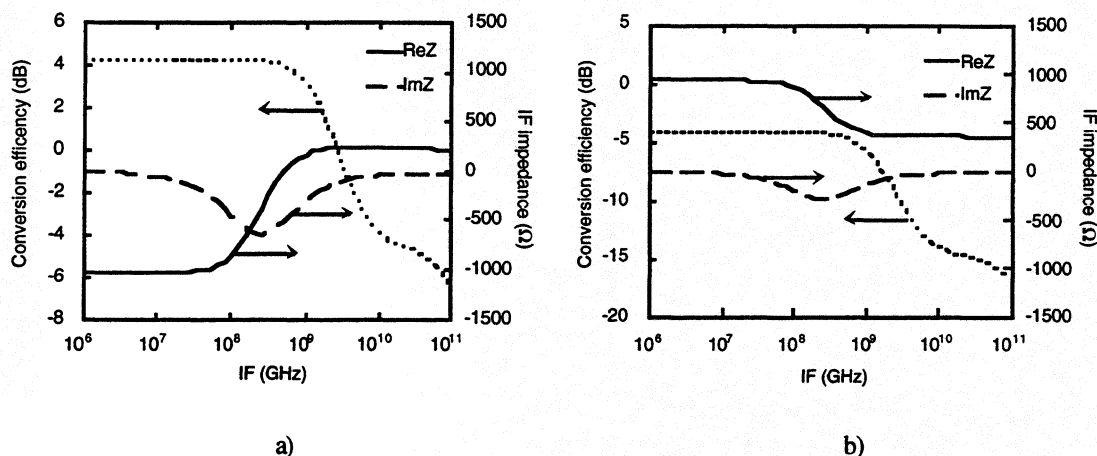
a)   b)

Fig. 6. Conversion efficiency vs IF and the IF impedance at two operating point :

a) minimum noise temperature (1100 K)

b) slightly higher LO power and noise temperature (1300K).

An increase of the operating temperature T causes a degradation of the mixer noise temperature because of a decrease of the optimal LO power. A set of parameters for $T = 77$ K is given in Table 2 (point 3). One can see the minimum noise temperature is ≈ 3 times higher than for $T = 66$ K. An advantage, however, is that the differential resistance at the optimum point is positive.

Table 2. Parameters of the mixer at different operating points.

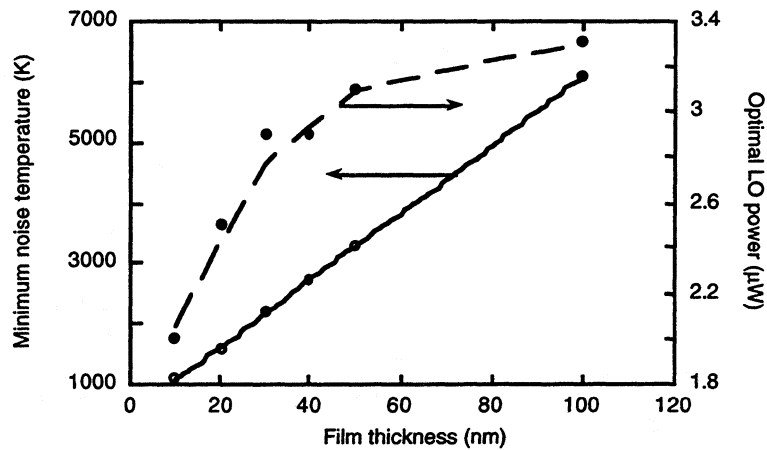| Point	T_M, K	P_{LO}, µW	P_{dc}, nW	R, Ω	η, dB	Z_0, Ω	Z(2.5GHz), Ω	T_e, K
1	1100	1.9	20	187	0.36	-1000	234-126j	84.9
2	1300	2.0	20	329	-9.3	936	367-60j	85.8
3	3000	0.7	10	195	-4.7	1600	225-61j	85

Fig. 7. Thickness dependence of the mixer noise temperature and optimal LO power.

VI. Conclusion.

We have developed a comprehensive model of thermal processes in a high-T_c HEB mixer. It was shown that the heat conductance from electron to phonons and escape of phonons through the film/substrate interface are the most critical processes in determining the device response and sensitivity. Using a two-temperature model, all important mixer parameters were calculated and studied for a practical range of conditions needed for a 2.5 THz heterodyne receiver for OH measurements. The effects of device size and of heat sink temperature have been evaluated. It was demonstrated that a submicron-size device made of a 10 nm thick film can have a very low noise temperature (~ 1000 K) and require only microwatts of LO power. These combination of parameters are very favorable for space-borne heterodyne instruments operating at terahertz frequencies

The research described in this paper was performed by the Center for Space Microelectronics Technology, Jet Propulsion Laboratory, California Institute of Technology, and was sponsored by the National Aeronautics and Space Administration, Office of Mission to Planet Earth, and the Office of Space Access and Technology.

References.

[1]. A. Skalare, W.R. McGrath, B. Bumble, H.G. LeDuc, P.J. Burke, A.A. Verheijen, and D.E. Prober, *IEEE Trans. Appl. Superconductivity* **5**, 2236 (1995).

[2]. T. Wang, K.M. Beauchamp, D.D. Berkley, B.R. Johnson, J.-X. Liu, J. Zhang, and A.M. Goldman, *Phys.Rev.B* **43**, 8623 (1991).

[3]. T. Terashima, K. Shimura, Y. Bando, Y. Matsuda, A. Fujiyama, and S. Komiyama, *Phys.Rev.Lett.* **67**, 1362 (1991).

[4]. J.-M. Triscone, Ø. Fischer, O. Brunner, L. Antognazza, and A.D. Kent, *Phys.Rev.Lett.* **67**, 804 (1990).

[5]. X.X. Xi, J. Greek, G. Linker, Q. Li, and O. Meyer, *Appl.Phys.Lett.* **54**, 2367 (1989).

[6]. J. Gao, B. Hänser, and H. Rogalla, *J.Appl.Phys.* **67**, 2512 (1990).

[7]. W.P. Shen, C. Lehane, J.P. Zheng, and H.S. Kwok, *Appl.Phys.Lett.* **64**, 3175 (1994).

[8]. J. Schneider, M. Mück, and R. Wördenweber, *Appl.Phys.Lett.* **65**, 2475 (1994).

[9]. J. Schneider, H. Kohlstedt, and R. Wördenweber, *Appl.Phys.Lett.* **63**, 2426 1993).

[10]. A.J.M. van der Harg, E. van der Drift and P. Hadley, *IEEE Trans.Appl.Superconductivity* **5**, 1448 (1995).

[11]. M.V. Pedyash, G.J. Gerritsma, D.H.A. Blank, and H. Rogalla, *IEEE Trans. Appl. Superconductivity* **5**, 1387 (1995).

[12]. H. Assink, A.J.M. v.d. Harg, C.M. Schep, N.Y. Chen, D. v.d. Marel, P. Hadley, E.M.J.M. v.d. Drift, and J.E. Mooij, *IEEE Trans.Appl.Superconductivity* **3**, 2983 (1993).

[13]. A.D. Semenov, R.S. Nebosis, Yu.P. Gousev, M.A. Heisinger, and K.F. Renk, *Phys.Rev.B* **52**, 581 (1995).

[14]. M. Lindgren, V. Trifonov, M. Zorin, M. Danerud, D. Winkler, B.S. Karasik, G.N. Gol'tsman, E.M. Gershenzon, *Appl.Phys.Lett.* **64**, 3036 (1994).

[15]. M. Danerud, D. Winkler, M. Lindgren, M. Zorin, V. Trifonov, B.S. Karasik, G.N. Gol'tsman, E.M. Gershenzon, *J.Appl.Phys.* **76**, 1902 (1994).

[16]. C.D. Marshall, I.M. Fishman, R.C. Dorfman, C.B. Eom, and M.D. Fayer, *Phys.Rev.B* **45**, 10009 (1992).

583

[17]. A.V. Sergeev, A.D. Semenov, P. Kouminov, V. Trifonov, I.G. Goghidze, B.S. Karasik, G.N. Gol'tsman, E.M. Gershenzon, *Phys.Rev.B* **49**, 9091 (1994).

[18]. G.L. Carr, M. Quijada, D.B. Tanner, C.J. Hishumugl, G.P. Williams, S. Estemand, B. Dutta, F. DeRosa, A. Inam, T. Venkatesan, and X. Xi, *Appl.Phys.Lett.* **57**, 2725 (1990).

[19]. N. Bluzer, *Phys.Rev.B* **44**, 10222 (1991).

[20]. Q. Hu and P.L. Richards, *Appl.Phys.Lett.* **55**, 2444 (1989).

[21]. M. Lindgren, M.A. Zorin, V. Trifonov, M. Danerud, D. Winkler, B.S. Karasik, G.N. Gol'tsman, and E.M. Gershenzon, *Appl.Phys.Lett.*, **65**, 3398 (1994).

[22]. N.Perrin and C. Vanneste, *Phys.Rev.B* **28**, 5150 (1983).

[23]. V.A. Trifonov, B.S. Karasik, M.A. Zorin, G.N. Gol'tsman, E.M. Gershenzon, M. Lindgren, M. Danerud, and D. Winkler, *this issue.*

[24]. E.M. Gershenzon, G.N. Gol'tsman, A.D. Semenov, and A.V. Sergeev, *Solid State Commun.* **76**, 493 (1990).

[25]. H. Ekström, B.S. Karasik, E. Kollberg, and K.S. Yngvesson, *IEEE Trans. on Microwave Theory and Techniques* **43**, 938π (1995).

[26]. B.S. Karasik and A.I. Elantev, *Appl.Phys.Lett.* **68**, 853 (1996); *Proc. 6th Int.Symp. on Space Terahertz Technology*, 21-23 March 1995, Caltech, Pasadena, pp. 229-246.

[27]. J.C. Mather, *Appl.Opt.* **21**, 1125 (1982).